The Journal of Comparative Neurology 517:512–523 (2009)
Research in Systems Neuroscience

Increased Levels of NMDA Receptor NR2A Subunits at Pre- and Postsynaptic Sites of the Hippocampal CA1: An Early Response to Conditional Double Knockout of Presenilin 1 and 2

CHIYE AOKI,[1]* JOYCE LEE,[1] HERMINA NEDELESCU,[1] TUNAZZINA AHMED,[1] ANGELA HO,[2] AND JIE SHEN[2]
[1]Center for Neural Science, New York University, New York, NY 10003
[2]Center for Neurologic Diseases, Brigham and Women's Hospital, Program in Neuroscience, Harvard Medical School, Boston, MA 02115

ABSTRACT

Greater than 90% of familial Alzheimer's disease (AD) is linked to mutations of presenilin (PS), and the loss of PS function altogether within mouse brains by conditional double knockout of the PS 1 and 2 genes (PS-cDKO) leads to age-dependent emergence of AD phenotypes, including neurodegeneration and reduced synaptic plasticity in the hippocampal CA1. The goal of our study was to identify the ultrastructural and molecular changes at synapses in the hippocampal CA1 of this PS-cDKO mouse model of AD. We examined the asymmetric (excitatory) synapses formed on apical dendrites of CA1 pyramidal neurons at 2 months postnatal, an age when AD-like symptoms emerge but brain morphology, as assessed by light microscopy, is still normal. Our quantitative electron microscopic analyses confirm that PS-cDKO hippocampi at 2 months postnatal do not yet exhibit synapse losses or spine size alterations. However, immunocytochemistry reveals that the same region exhibits a 28% increase in the proportion of spines labeled for the NR2A subunits of NMDA receptors (NMDAR), with a 31% increase specifically at postsynaptic densities and a concomitant reduction of these subunits at nonsynaptic sites within spine heads. In contrast, no change in levels or the distribution pattern of NR2B subunit levels were detected within spine heads. Presynaptically, NR2A levels are elevated at axo-spinous junctions and these may contribute to the timing-dependent, long-term depression. These observations point to an early-onset trapping of NMDAR at synapses that are subtle but may underlie the reduced synaptic plasticity at 2 months of age and excitotoxicity at later stages. J. Comp. Neurol. 517:512–523, 2009.

Indexing terms: synaptic plasticity; synapse density; electron microscopy; immunocytochemistry, Alzheimer's disease; CA1; hippocampus; neurodegeneration; mouse; animal model; NR2B

Extensive research has led to the hypothesis that cognitive impairments associated with the early phases of Alzheimer's disease (AD) is due to the loss of synaptic function (Selkoe, 2002; Counts et al., 2006), which only later is followed by neuronal loss (Zarow et al., 2003). Multiple candidates have been suggested as the culprit underlying the cause of AD (Hardy and Selkoe, 2002; Bezprozvanny and Mattson, 2008). Of these, presenilin (PS) dysfunction is a particularly prominent candidate, based on the observation that greater than 90% of the familial AD is linked to mutations of PS (Hutton and Hardy, 1997), and the loss of PS1 and PS2 function by conditional double knockout (PS-cDKO) is an animal model that phenocopies AD closely (Shen and Kelleher, 2007). The AD phenotypes exhibited by PS-cDKO include the reduction of long-term potentiation (LTP) and paired-pulse facilitation in the stratum radiatum of hippocampal CA1 and impairment of spatial memory acquisition (Shen and Kelleher, 2007). Initially, morphological changes are not detectable by light microscopy. However, by the sixth month, cortex and hippocampus of these animals exhibit accumulation of glial fibrillary acidic proteins, neurofibrillary tangles and hyperphosphorylated tau,

Grant sponsor: New York University's Challenge Fund; Grant sponsor: National Institutes of Health; Grant numbers: 2R01DA009618-10A1 (to C.A.), NS41783; Grant sponsor: Alzheimer's Association; Grant number: IIRG 07-58479 (to J.S.).

Joyce Lee, Hermina Nedelescu, and Tunazzina Ahmed contributed equally to this work.

*Correspondence to: C. Aoki, Center for Neural Science, New York University, New York, NY 10003. E-mail: ca3@nyu.edu

Received 4 March 2009; Revised 15 May 2009; Accepted 4 July 2009
DOI 10.1002/cne.22151
Published online July 17, 2009 in Wiley InterScience (www.interscience.wiley.com).

together with signatures of inflammation and neurodegeneration, including reductions of dendritic complexity and spine losses (Saura et al., 2004). These observations indicate that maintenance of healthy synaptic circuit relies on the presence of fully functional PS within brain. However, the reason why the loss of PS function leads to these AD phenotypes remains unclear. We wanted to answer the question, *How and why* the loss of PS function leads to these progressive, age-dependent changes. Knowledge of the molecular alterations occurring precisely at synapses (i.e., at synaptic membrane surfaces and postsynaptic densities [PSDs]) at the onset of the disease is likely to be useful for understanding the etiology of AD. To this end, we have taken the approach of electron microscopic immunocytochemistry (EM-ICC) to quantify the earliest changes in the levels of specific proteins precisely at synapses of intact brain tissue of PS-cDKO brains.

Within PS-cDKO brains, the loss of PS1 and 2 starts at around postnatal day 18. Deficits in hippocampus-dependent memory and hippocampal LTP emerge by the second postnatal month, many weeks prior to the appearance of overt morphological changes (Saura et al., 2004). So as to capture the earliest structural and molecular changes at synapses that may lead to AD-like symptoms, we examined the brains of PS-cDKO animals at 2 months postnatal. In this initial study, we focused our analysis on the localization of *N*-methyl-D-aspartic acid receptor (NMDAR) subunits at asymmetric (presumably excitatory) synapses in stratum radiatum of the CA1, because both of the deficits exhibited by these animals—i.e., the spatial memory task (the Morris water maze) and LTP—depend on NMDAR activity-dependent synaptic plasticity in the CA1 field of the hippocampus. In particular, we examined the localization of the NR2A and NR2B subunits, instead of the obligatory NR1 subunits, since the NR2A/B subunits confer synaptic localization of NMDARs (Tovar and Westbrook, 1999; Thomas et al., 2006).

Our quantitative EM-ICC analyses indicate that PS-cDKO tissue at this age exhibit no overt ultrastructural changes but that the levels of NR2A subunits of NMDA receptors are elevated within spines and specifically at the synaptic junction. These observations point to early changes in the distribution of NMDAR that are subtle but may lead to excitotoxicity at later ages.

MATERIALS AND METHODS

Generation of PS-cDKO mice was achieved at the animal facility at Harvard Medical School. We crossed floxed PS1 (fPS1), αCaMKII-Cre transgenic (Yu et al., 2001), and PS2−/− (Steiner et al., 1999) mice together to obtain fPS1/fPS1; αCaMKII-Cre; PS2−/− mice. Four PS-cDKO mice, derived from two litters, were used for the EM study. For controls, two genotypes of mice were used: one was the fPS1 (three mice), which were floxed but otherwise of the same genotype as wildtype (WT) and expressed both PS1 and PS2. The other control was the PS2−/− (two mice), from which the PS2 gene was deleted but the PS1 gene was retained. Neither of these controls exhibit histological abnormalities, as assessed by light microscopy. Their memory is also intact, based on the performance in the Morris water maze to assess spatial memory or contextual fear conditioning, used to assess associative memory (Saura et al., 2004). Importantly, none of the animals that underwent EM-ICC analyses had been used for behavioral studies antemortem, so as to avoid inducing any change in synaptic proteins as a consequence of experience.

Antibody information, antibody characterization, and related immunoreagents

The antibody directed against the NR2A subunit of NMDARs was purchased from Upstate Biotechnology (Lake Placid, NY, Cat. No. 07-632). The antibody was produced in rabbits and was directed against amino acids 1265–1464 of the C-terminus of mouse NR2A subunit. Specificity of this antibody has been demonstrated previously by Western blot (manufacturer's datasheet) and confirmed in subsequent publications (Rinaldi et al., 2007), which show that this antibody recognizes a single band corresponding to ≈170 kD, the molecular weight of NR2A subunits. The antibody directed against the NR2B subunit of NMDARs was produced in rabbits and directed to the C-terminal 20 amino acids of mouse NR2B (KFNGSSNGHVYEKLSSIESDV). This antibody was also purchased from Upstate Biotechnology (Cat. No. 06-600) and has been shown to not crossreact with the NR2A or NR1 subunits of NMDARs (Rinaldi et al., 2007). Previous EM-ICC studies determined that this antibody recognizes asymmetric synapses but not the symmetric synapses (Erisir and Harris, 2003; Fujisawa and Aoki, 2003; Kobayashi et al., 2007). That the NR2A and NR2B antibodies recognize distinct protein species was further verified, based on the observation that the levels of the NR2A and NR2B subunit at synapses change in opposite directions (NR2A levels rise, while the NR2B levels decline) following in vivo application of an NMDAR blocker, D-APV (Aoki et al., 2003; Fujisawa and Aoki, 2003).

Secondary antibodies used for the described studies were biotinylated antirabbit IgG produced in goat (from Vector Laboratories, Burlingame, CA, Elite kit, Cat. No. PK 6200) or gold-conjugated antirabbit IgG, produced in goat, for which the colloidal gold particles were 10 nm in diameter (Aurion, EM-Science, Fort Washington, PA, Cat. No. 810.011). Bovine serum albumin (BSA) was purchased from Sigma Chemicals (St. Louis, MO). Glutaraldehyde, osmium tetroxide, paraformaldehyde, and EMBED-812 were purchased from EMSciences. The Silver IntesEM kit was purchased from Amersham (Arlington Heights, IL, Cat. No. RPN 491).

Preparation of brain tissue for light and electron microscopy

Mice were euthanized by transcardial perfusion with fixatives at the laboratory of Jie Shen, Harvard Medical School, while the postmortem preparation of tissue for EM-ICC was performed in the laboratory of Chiye Aoki, New York University (NYU).

At the age of 8 weeks postnatal, mice were deeply anesthetized using Nembutal (50 mg/kg i.p.), then euthanized by transcardial perfusion with fixatives. A peristaltic pump was used to control the flowrate of the perfusates to 10–50 mL/min. The perfusates were the following: 1) 10–50 mL of saline containing heparin (1,000 U/mL), over a 1-minute period; 2) 200 mL of 4% paraformaldehyde in 0.1 M phosphate buffer (PB, pH 7.4). No other aldehydes were added to the perfusate. This omission was intentional, to avoid overfixation of the tissue during the shipment from Harvard to NYU. Previous studies have shown that tissue postfixed with glutaraldehyde after the immunocytochemical procedure but before fixation with osmium tetroxide provides adequate preservation of ul-

trastructure and antigenicity for most immunocytochemical procedures.

All steps of this procedure were in accordance with the protocol approved by the University Animal Welfare Committee of Harvard Medical School and in full conformance with the recommendations of the 1996 edition of the NIH *Guide for the Care and Use of Laboratory Animals* and all applicable Federal, State, and local laws, and as outlined in the NIH the principles for use of animal (NIH Manual Chapter 4206).

Following this perfusion, brains were removed from the skull, then immersed in the same fixative while shipped on ice to the Aoki laboratory at NYU. Within 1 day following the perfusion, the brain was cut into 40-μm-thick coronal sections using a vibratome. Subsequently, the sections were stored for up to 1 month, free-floating at 4°C in 0.01 M PB with 0.9% sodium chloride (PBS, set to pH 7.4) containing 0.05% sodium azide.

NR2A/NR2B immunocytochemistry and the rationale for the use of the two immunolabels

Immunocytochemistry was performed to immunolabel the NR2A subunits of NMDAR using two EM-ICC procedures as described previously (Aoki et al., 2000). In brief, the HRP-DAB procedure was used to optimize detection of immunolabels within spines. Immunolabels were applied on free-floating vibratome sections, prior to embedding in the plastic resin, EM812, using 3,3′-diaminobenzidine and H_2O_2 as substrates (HRP-DAB). The NR2A antibody was used at a concentration of 1 μg/mL, incubated overnight at room temperature under constant agitation, using PBS (pH 7.6) as a diluent, together with 1% BSA and 0.05% sodium azide. Following this incubation, sections were rinsed in PBS for 1 hour at room temperature, then immersed in the secondary antibody solution. The secondary antibody, goat antirabbit IgG, was applied to the sections for 1 hour at room temperature under constant agitation at a dilution of 1:100, using PBS-BSA with 0.05% sodium azide as the diluent. The avidin-biotin-peroxidase complex was prepared according to the manufacturer's specifications—i.e., by suspending 2 drops of solution A and 2 drops of solution B in 5 mL of PBS over a period of 30 minutes prior to application. After rinsing the vibratome sections in PBS, the sections were incubated in this ABC solution for 30 minutes, then rinsed in PBS, before immersing them in the HRP substrate of 3,3′-diaminobenzidine and H_2O_2. The HRP reaction was allowed to proceed for 10 minutes and terminated by rinsing the sections in PBS. The HRP-DAB labeled sections were postfixed with 1% glutaraldehyde and 1% osmium tetroxide. All of these steps were performed identically for all of the sections collected from the control and PS-cDKO brains, by performing all steps of the ABC reaction strictly in parallel, so as to ensure that all immunoreagents, incubation periods, rinses, and HRP-reaction times were identical.

The other immunolabeling procedure was PEG (postembed immunogold labeling), used to quantify the level of immunolabeling directly over the postsynaptic densities (PSDs) versus other sites within spine heads that are removed from the PSD. Vibratome sections designated for this procedure were fixed in the absence of osmium tetroxide (Phend et al., 1995) so as to retain antigenicity of NR2As. The tissue was embedded in EPON812, and the ultrathin sections were processed with modifications described specifically for PEG-labeling of NR2A subunits (Erisir and Harris, 2003). Specifically, the concentration of the anti-NR2A antibody was 10 μg/mL, while the concentration of the secondary antibodies—10 nm gold-conjugated antirabbit IgG antibodies—was 1:100. As described for the HRP-DAB-labeled material, all of the PEG procedures for all ultrathin sections were performed in parallel, so as to ensure that all reagents, incubation periods, and rinses were performed identically across the control and PS-cDKO tissue.

The NR2B subunit of NMDARs was also probed within spines by the same PEG procedure, but using the anti-NR2B antibody at a concentration of 10 μg/mL.

Immunocytochemical controls

Each EM-ICC procedure was accompanied by controls. These consisted of the verification that omission of the primary antibody or use of secondary antibodies that were mismatched for species yielded no immunolabeling that could be detected by light or electron microscopy. To verify the extent of background labeling by the PEG procedure, we sampled 400 asymmetric synapses from two control and two PS-cDKO hippocampi and tallied the frequency of PEG located at synapses. In the absence of the primary antibody, only one exhibited PEG labeling over the postsynaptic density and two exhibited PEG labeling at the presynaptic membrane. The remaining synapses exhibited no PEG labeling at all. Besides these controls, electron microscopic examination revealed that, in the presence of primary antibodies, the NR2A or NR2B-immunolabeling of the hippocampus of PS-cDKO and control brains never occurred postsynaptic to symmetric (presumably inhibitory) synapses, as was observed previously in rodent brain tissue (Erisir and Harris, 2003; Fujisawa and Aoki, 2003; Kobayashi et al., 2007), thereby indicating specificity of labeling at the subsynaptic level and in a pathway-specific manner.

Digital capturing of electron microscopic images and areas sampled

All persons capturing images were kept blind to the genotype of the animal, so as to eliminate bias in sampling of neuropil. Images used for quantitative analyses were captured digitally using a Hamamatsu CCD camera and software developed by AMT (Boston, MA), attached to a JEOL 1200XL electron microscope. Images were digitally captured at a magnification of 50,000× for PEG-immunolabeled tissue, 40,000× for HRP-DAB immunolabeled tissue, and at 20,000× for synapse density analysis. The anatomical region was verified to be the stratum radiatum in the CA1 field of the hippocampus by sweeping the ultrathin sections at a magnification of 4,500×. At this magnification, immunolabeling cannot be resolved. This magnification was chosen so that our choice of the region to be sampled would not be biased by the level of overall immunolabeling.

All micrographs used for quantitative analyses were taken from regions of the neuropil that fulfilled the following criteria. 1) The neuropil resided approximately midway within stratum radiatum of CA1 within the dorsal blade of the hippocampus. This anatomical region was displaced from the base of the pyramidal cell layer by at least 50 μm and was also removed from stratum lacunosum-moleculare by $\approx$50 μm. Under the electron microscope, it was evident that the middle portion of stratum radiatum was clearly removed from the portion of the

neuropil traversed by the large, proximal portions of the apical dendrites of CA1 pyramidal neurons. 2) For the HRP-DAB-labeled tissue, only the neuropil was required to reside within portions of vibratome sections forming the razor-blade-cut surface, where penetration of immunoreagents into the vibratome sections would be maximal. For PEG-immunolabeled tissue, the neuropil resided within portions of vibratome sections that were removed from the surface, so as to avoid sampling of neuronal profiles that were less than the full thickness of the ultrathin sections. For both labeling approaches, sampling of stratum radiatum spanned multiple ultrathin sections collected on multiple grids and traversing distances greater than 200 μm laterally and at least 100 μm dorsoventrally.

Quantitative electron microscopic analyses

For all parts of the quantitative analyses that were performed offline, the person performing the tallying was kept blind to the genotype of the animal. Systematic sweeps were made across the tissue to digitally capture the synaptic neuropil. Within 2D digitized images, synapses were identified as asymmetric and Gray type 1, based on the presence of thick PSDs that aligned the intracellular surfaces of plasma membranes abutting vesicle-filled axon terminals. These asymmetric (presumably excitatory; Kennedy and Ehlers, 2006) synapses were numbered in the order encountered. Each asymmetric synapse was subsequently categorized as being associated with or without NR2A or NR2B immunolabel. On some of the images the contrast of the digital image was varied to facilitate detection of NR2A/B labels that resided directly over the PSD using Adobe Photoshop (v. 7.0, San Jose, CA).

For HRP-DAB and especially for the PEG-labeled tissue, the immunolabeling was sufficiently discrete to allow discrimination of the immunoreactive sites as synaptic or nonsynaptic. For PEG-labeled tissue, the position of immunolabel was categorized as being at the PSD, if the immunolabeling was directly over the PSD ('at PSD') or in the synaptic cleft. These categorizations correspond to Bins 1–3 and 5, respectively, of Yildirim et al. (2008). Labeling that occurred within a distance equal to twice the thickness of the PSD in its plane of section were categorized as 'near PSD,' while those within the spine head but removed from the PSD by a distance greater than twice the thickness of the PSD was categorized as nonsynaptic but 'In Spine.' Our 'Near PSD' and 'In Spine' categories together correspond to Bin 4 of Yildirim et al. (2008). Figure 4 shows examples of all of these postsynaptic positions with respect to PSDs. Labeling on the presynaptic side was also categorized as being "at the presynaptic membrane" (Bin 6 of Yildirim et al., 2008), "near the presynaptic membrane" (Bin 7) or "within the axon terminal but removed from the presynaptic membrane" (Bin 8). Total presynaptic axon terminal labeling was determined by combining the tallies from all three regions within axon terminals. The pre- and postsynaptic immunoreactive zones are schematized in Figure 1.

To quantify the frequency of immunolabeling for NR2A labeling, an equal number of synapses were analyzed from each animal. For the HRP-DAB-labeled material, the number of synapses associated with immunolabel was tallied for every group of 10 synapses that were encountered. This tallying was repeated exactly 11 times for each animal (i.e., reflecting analysis of 110 synapses per animal, and repeated for each of the five control genotype brains and four PS-cDKO brains). The mean and standard error of the mean (SEM) of the percent of labeled synapses (per 10 synapses) for each genotype group were calculated and subjected to the unpaired *t*-test. The *n*-value used for statistics was 55 for the controls (11 tallies per animal × 5 animals) and 44 for the PS-cDKO tissue (11 tallies per animal × 4 animals).

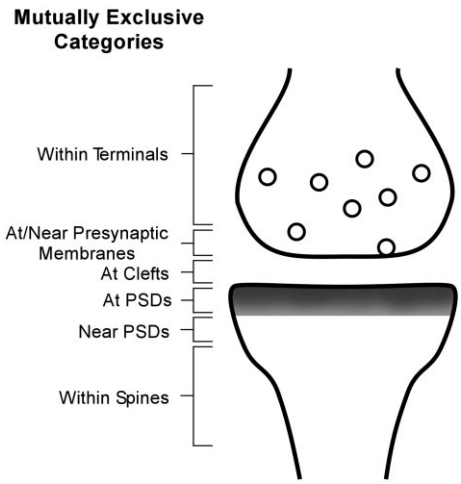

Figure 1.
Cartoon depicting the categories of PEG-locations used to compare the distribution of NR2A- and NR2B-immunoreactivity in the vicinity of asymmetric (presumably excitatory) synapses in the CA1 field of the hippocampus.

For PEG-labeled tissue, quantification was performed by determining the average number of particles per single synapse. Exactly 200 synapses were analyzed from each animal's hippocampal tissue. Although all five of the control genotype brain tissue underwent NR2A PEG, only three were later confirmed to have been in the stratum radiatum of the CA1 field of the hippocampus. Therefore, only 600 synapses (200 synapses × 3 animals) were used to calculate the mean and SEM values and statistical analyses. All four of the PS-cDKO brains underwent the PEG labeling in parallel with the control samples and all four were confirmed to have been from the stratum radiatum of the CA1. Therefore, the *n*-value for the analysis derived from the PEG analysis was 800 (200 synapses per brain × 4 PS-cDKO brains) for the PS-cDKO tissue. For NR2A-labeling by the PEG procedure, we analyzed the PEG localization one step further. Specifically, the labeling at the PSD was divided into those within Bin 1, as defined by Yildirim et al.—i.e., within 30 nm from the inner surface of the synaptic plasma membrane, versus those in Bin 2—residing 30–60 nm from the inner surface of the synaptic membrane.

Analysis of the frequency of encounter with synapses per unit area

The ultrathin sections prepared to determine NR2A-immunoreactivity were reexamined and recaptured digitally at a lower magnification (20,000×) to determine the frequency of encounter with synaptic profile within ultrathin sections collected from the stratum radiatum of the CA1 field. Synapse encounter frequency was determined by calculating the mean of the number of synaptic profiles captured in each electron

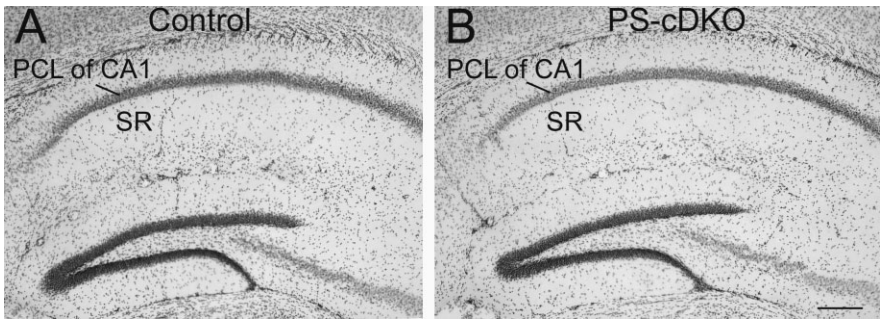

Figure 2.
Light micrographs demonstrate nearly identical cell packing pattern in the hippocampus across the control **(A)** and PS-cDKO **(B)** genotypes. The sections were Nissl stained. PCL, pyramidal cell layer; SR, stratum radiatum. Scale bar = 200 μm.

micrograph (45.385 μm^2 per micrograph). The electron micrographs were taken by sweeping systematically from a zone where the pyramidal cell bodies disappeared (pyramidal cell layer, PCL) and up to the hippocampal fissure, just beyond the stratum lacunosum moleculare (SLM). The number of micrographs needed to tile from the stratum radiatum from the PCL to the SLM ranged from 19–31 per animal (938–1,539 μm^2). Portions of the neuropil containing blood vessels or somata were excluded from synapse encounter frequency calculations using Image J (NIH, Bethesda, MD) to estimate such areas. Portions of the ultrathin sections containing no neuropil (i.e., EPON resin only) were also excluded for calculating synapse encounter frequency. Since the synapse encounter frequency varied 4-fold within any single animal's stratum radiatum in a fashion that was strongly influenced by the laminar position, relative to the PCL and SLM (Fig. 7), six consecutively collected micrographs positioned roughly equidistant from the PCL and SLM ($\approx$60 μm from either strata) were used to derive the mean and SEM of synapses per unit area for each animal, and the average values of each animal were compared across genotypes.

Statistical analyses

All statistical analyses were performed using the software Statistica (v. 6.0, Statsoft, Tulsa, OK) and confirmed using another software, SPSS (v. 15.0, Chicago, IL). When comparing data across the two genotypes, Student's *t*-test was used. Significance was accepted for *P*-values less than 0.05.

Capturing and reproduction of figures

Electron microscopic images were captured and stored using the CCD camera attached to a JEOL 1200XL via software developed by AMT. Light microscopic images were captured at a magnification of 5× using a CCD camera attached to a Zeiss Axiophot microscope. For reproduction, a subset of these images were adjusted in contrast, brightness, and image size using Adobe Photoshop (v. 7.0).

RESULTS

LM reveals no overt difference in the hippocampus of control and PS-cDKO

Previous studies have indicated that PS-cDKO brains exhibit signs of inflammation and neurodegeneration but that these changes are not yet apparent at 2 months of age (Saura et al., 2004). Light microscopy was performed to determine whether any changes might be detectable by Nissl staining. As expected, no overt difference was noted (Fig. 2).

EM-ICC using HRP-DAB labels reveals an augmentation of the proportion of spines immunoreactive for the NR2A subunits within PS-cDKO hippocampi

At 2 months of age, mice lacking both PS1 and PS2 exhibit impairment in spatial memory, as assessed by the increased escape latency and path lengths that these animals exhibit in finding the hidden platform of the Morris water maze. These behaviors were categorized as mild memory impairment, since the animals still exhibit improvements in their performance over the course of 5 training days (Saura et al., 2004). To determine whether this mild form of spatial memory impairment could be due to decreased levels of NMDARs at synapses of the hippocampus, the asymmetric synapses formed on apical dendrites of the CA1 pyramidal neurons were assessed for the presence of the NR2A and NR2B subunits of NMDARs.

HRP-DAB was used so as to optimize detection of immunoreactivity anywhere within dendritic spines in stratum radiatum of the CA1 field of four PS-cDKO and five age-matched control animals. EM-ICC revealed that both the control and PS-cDKO brains exhibit NR2A immunolabeling along thick PSDs and at plasmalemmal sites within spines that are removed from the active zone (Fig. 3). In contrast, symmetric synapses with thin PSDs were devoid of immunoreactivity, as were many thick PSDs in the immediate vicinity.

Quantification of the population of asymmetric synapses within the stratum radiatum of CA1 (110 per animal, altogether 550 from control tissue and 440 from PS-cDKO tissue) exhibiting NR2A-immunoreactivity revealed that NR2A immunolabeling is not reduced within the hippocampus of PS-cDKO mice. On the contrary, the proportion of asymmetric synapses immunolabeled for NR2A is augmented by 28% within the hippocampus of PS-cDKO mice, relative to the hippocampus of controls ($P < 0.05$; unpaired *t*-test, *t*-value = −2.34; Fig. 3A).

PEG reveals augmentation of NR2As at the PSD of PS-cDKO hippocampi

Even though the proportion of asymmetric synapses immunoreactive for NR2A was higher for the hippocampus of PS-

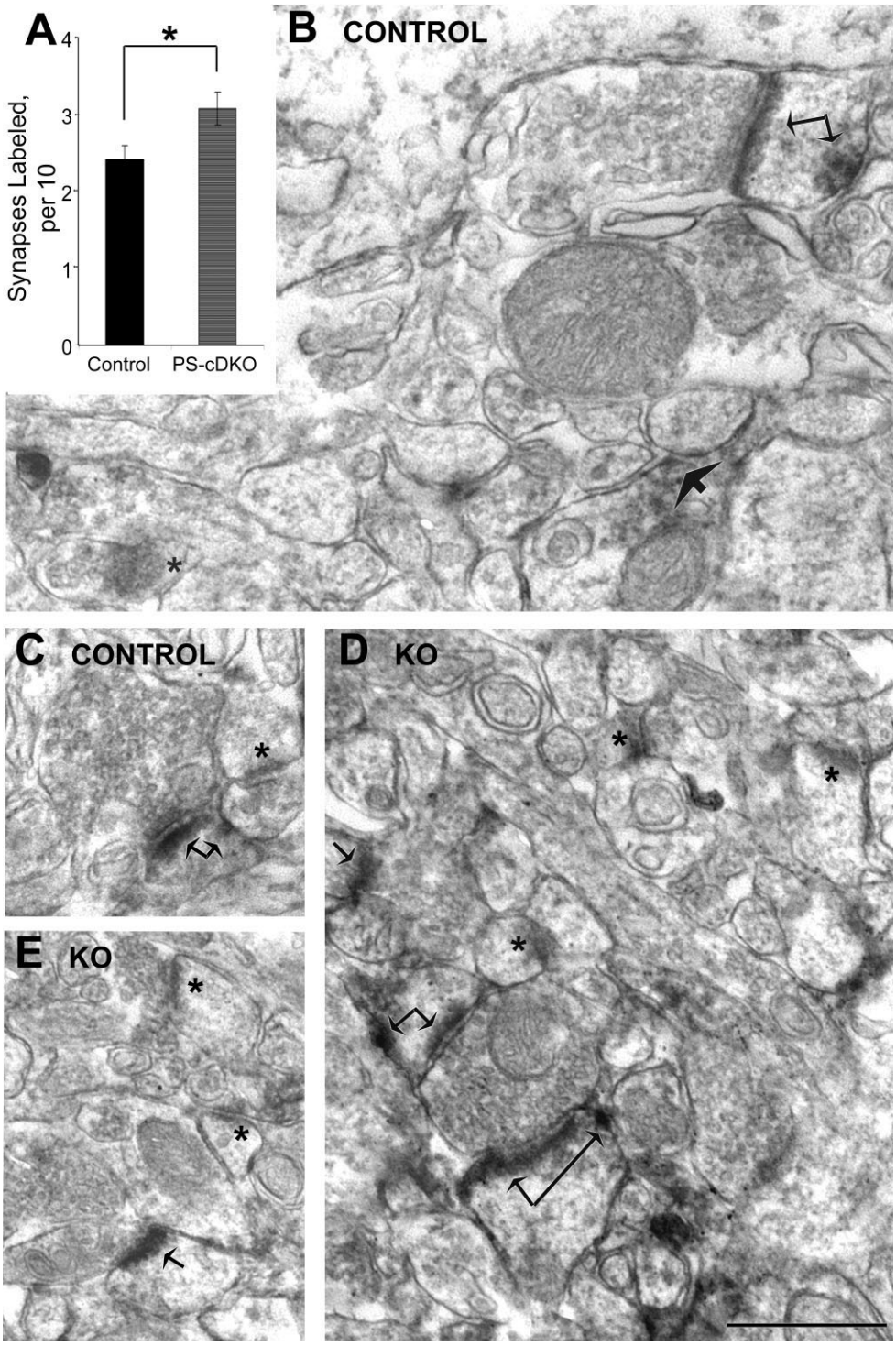

Figure 3.
HRP-DAB reveals augmentation of PS-cDKO spines containing NR2A. Micrographs **(B–E)** show examples of asymmetric synapses immunolabeled for the NR2A subunit of NMDARs, using the HRP-DAB label. Arrows point to labels accumulating along the plasma membrane. Double-arrows point to spines immunolabeled at both the synaptic and nonsynaptic portions of dendritic spines. Asterisks indicate PSDs that lack detectable levels of HRP-DAB. The bar graph **(A)** summarizes the quantitative analysis, indicating that the proportion of synapses immunolabeled for NR2A by HRP-DAB is significantly greater for the PS-cDKO hippocampus, relative to values obtained from age-matched control hippocampus. Electron micrographs from five control animals and three PS-cDKO animals were analyzed. From each animal, 110 synapses were analyzed strictly in the order that they were encountered during the random visual sweeping of the ultrathin section. For every group of 10 synapses the proportion of synapses labeled was assessed. This assessment was repeated exactly 11 times (10 synapses/assessment × 11 assessments = 110 synapses). Therefore, the *n*-value was 55 for the control group (550 synapses analyzed) and 44 for the PS-cDKO group (440 synapses analyzed). Asterisk indicates $P < 0.05$. Scale bar = 500 nm.

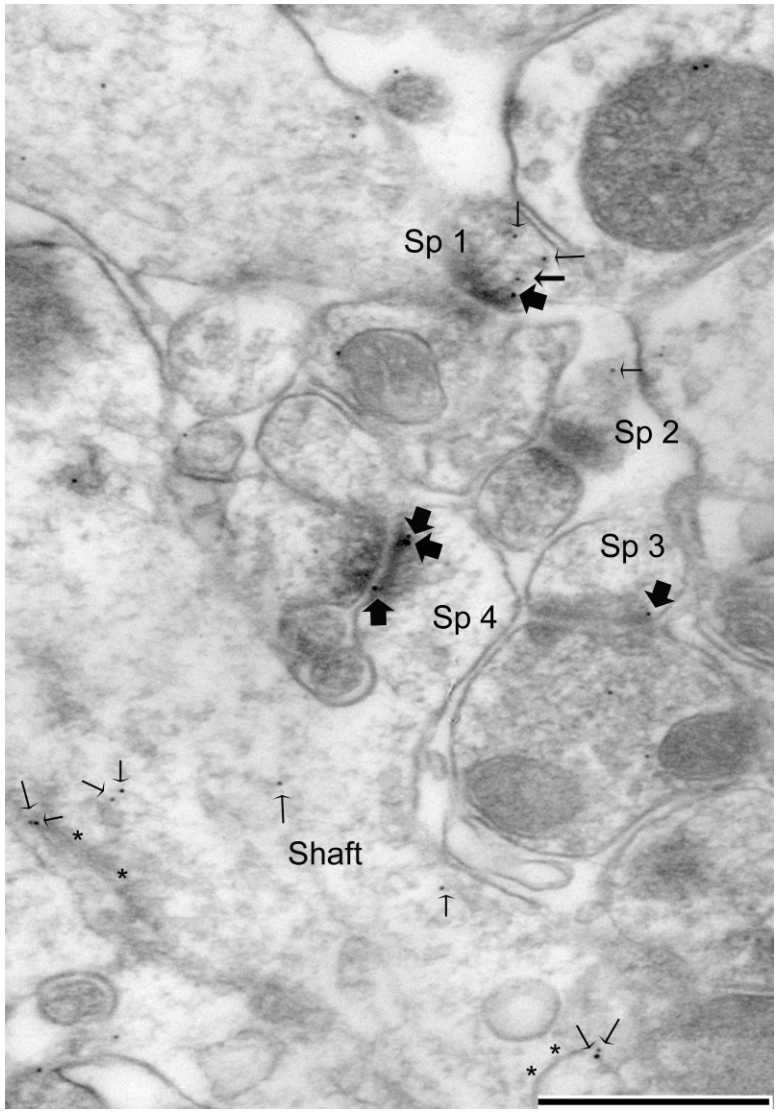

Figure 4.
PEG reveals NR2A at the PSD and nonsynaptic sites within spines of the hippocampus. The micrograph shows an example of NR2A-immunolabel tallying in stratum radiatum of the CA1 field. This particular example was taken from a PS-cDKO animal's tissue. Spines 1, 3, and 4 exhibit immunolabeling directly over the PSDs (largest arrows). Spine 1 also exhibits immunolabeling that is near but not directly over the PSD (intermediate size arrow). Here and elsewhere, small-sized arrows point to nonsynaptic immunolabeling, some of which occur in the spine head (Sp 1 and 2) and others in the dendritic shaft, near membranes of smooth endoplasmic reticulum (asterisks). Scale bar = 500 nm.

cDKO mice than of control mice, the possibility remained that the level of NR2A located precisely at the postsynaptic membrane of each synapse is less. To unambiguously identify synaptic versus nonsynaptic NR2A, the PEG procedure was employed. Using the PEG procedure, NR2A immunoreactivity was detected clearly over thick PSDs (large arrows in Fig. 4). PEG particles also occurred within the synaptic cleft or spine cytoplasm but still in the vicinity of PSDs (less than a distance equal to the thickness of PSDs) (intermediate size arrow in Fig. 4). PEG particles occurring within these subregions of the synapse were considered "synaptic," as these are distances expected to be generated by colloidal gold binding to antigens through primary antibody / secondary antibody bridges. PEG particles also occurred clearly removed from the PSDs (by distances greater than the thickness of PSDs, ≈60 nm) (smallest arrows in Fig. 4). PEG particles residing at sites removed from PSD by distances greater than the thickness of PSDs were categorized as nonsynaptic. As was observed within HRP-DAB-labeled tissue, some of the thick PSDs in the immediate vicinity lacked associations with PEG particles. PEG particles were consistently absent from symmetric synapses and entirely absent within tissues that underwent the PEG procedure but in the absence of the primary antibodies. Specifically, of 400 asymmetric synapses sampled from control and PS-cDKO tissue, only 1 PEG particle occurred postsynaptically.

Even by the PEG procedure, the level of NR2A residing at and near the PSDs and in the cleft was greater by 19% for the

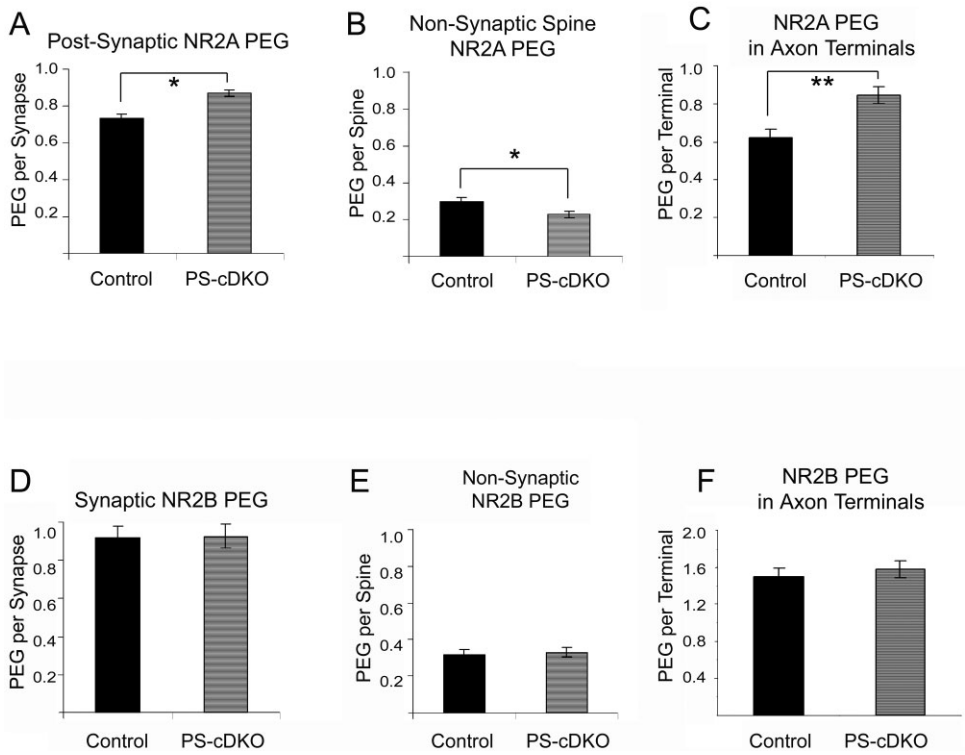

Figure 5.
NR2A is elevated both pre- and postsynaptically in the PS-cDKO hippocampus but NR2B levels are unchanged. For the NR2A-subunit analysis, synapses from three control animals and four PS-cDKO animals were analyzed, sampling exactly 200 synapses from each animal. Therefore, the *n*-value was 600 for the controls and 800 for the PS-cDKO group. PEG quantification reveals that NR2A subunits are significantly elevated at and near the PSD **(A)** and in presynaptic axon terminals **(C)**. In contrast, the NR2A labeling is significantly reduced at sites removed from the PSD of spines in the CA1 of PS-cDKO brains **(B)**. $*P < 0.05$; $**P < 0.0005$. Analysis of NR2B immunolabeling was performed across synapses from four control animals and four PS-cDKO animals. Exactly 100 synapses were sampled from each animal. Therefore, the *n*-value was 400 for both groups. The NR2B-PEG analysis revealed no difference at postsynaptic **(D)**, presynaptic **(F)** or nonsynaptic **(E)** domains of asymmetric synapses.

CA1 of hippocampus of PS-cDKO brains, relative to those of control (Fig. 5A). This difference was statistically significant ($P < 0.05$, $t = -2.40$, unpaired *t*-test). Further analysis of the synaptic NR2A-labeling revealed that the difference across genotypes resided precisely within the region of synapses that are 0–30 nm from the intracellular surface of the plasma membrane (Bin 1 of Yildirim et al., 2008). In this region the PEG level was 31% higher for the PS-cDKO synapses, relative to control synapses, and this difference was statistically significant ($P = 0.006$, $t = -2.74$). In contrast, NR2A labeling in Bin 2 (30–60 nm from the postsynaptic membrane) was much less than in Bin 1 (0.10 ± 0.02 for controls; 0.13 ± 0.02 for PS-cDKO) and not significantly different across the two genotypes ($P = 0.21$, $t = -1.26$).

The levels of nonsynaptic NR2As, as assessed by counting the PEG particles residing within spines but removed from PSDs, differed across the two genotypes but in the opposite direction. PEG particles were fewer at nonsynaptic sites within spines of PS-cDKO synapses relative to controls. Even after normalizing for the overall levels of PEG particles within postsynaptic spines, the levels of PEG at nonsynaptic sites was reduced by 24% in the PS-cDKO CA1 (*t*-value = 2.57; $P < 0.05$; Fig. 5B). Importantly, the average total PEG level within postsynaptic spines (synaptic plus nonsynaptic) was not significantly different across the two genotypes (*t*-value = −1.22; $P = 0.22$).

NR2B levels at synapses of PS-cDKO hippocampi remain unchanged

In the hippocampus, NMDARs can occur as heteromers with NR2B subunits. To determine whether PS-cDKO leads to reduction of NR2B subunits, spines of the same hippocampal tissue were immunolabeled for the NR2B subunits. EM-ICC revealed that NR2B subunits also occur synaptically and nonsynaptically and are more prevalent presynaptically than are the NR2A-subunits (Fig. 6). Analysis of 800 synapses residing within the CA1 field of four PS-cDKO and four control animals (i.e., 200 synapses per animal) revealed that NR2B levels are identical across the two groups, both at synapses (unpaired *t*-test, *t*-value = −0.085, $P = 0.932$) and at nonsynaptic sites within spines (Fig. 5D,E) (unpaired *t*-test *t*-value = −0.364; $P = 0.717$).

Presynaptic NR2A and NR2B

Previous EM-ICC localization studies have shown that NMDAR subunits occur presynaptically (Aoki et al., 1994, 2003; Corlew et al., 2007), and play a strong modulatory role on synaptic plasticity through regulation of glutamate release.

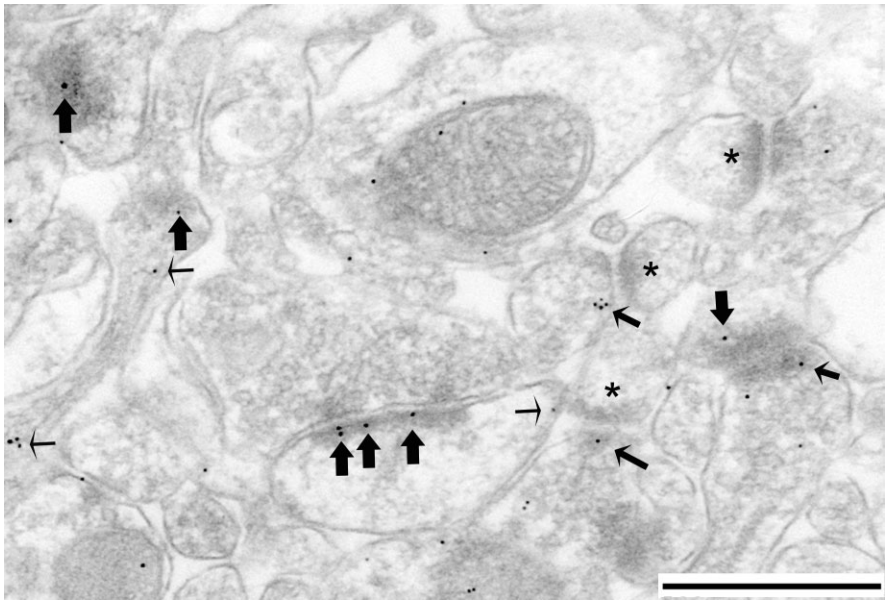

Figure 6.
NR2B PEG labeling occurs both pre- and postsynaptically. NR2B-PEG quantification was performed using electron micrographs such as the one shown here, taken from stratum radiatum of a PS-cDKO brain. Large arrows point to postsynaptic labeling, while small arrows point to nonsynaptic labeling within spines. Intermediate size arrows point to presynaptic labeling. Asterisks point to unlabeled PSDs. Scale bar = 500 nm.

We therefore extended our PEG analysis to presynaptic axon terminals. The results indicated a pattern parallel to that described for the postsynaptic NR2 subunits, namely, a 36% increase of NR2A subunits within axon terminals forming asymmetric synapses onto dendritic spines of the PS-cDKO hippocampus, relative to the frequency observed for age-matched controls (Fig. 5C) (t-value = −3.632; $P < 0.0005$). No difference in the presynaptic NR2B levels was detected across the two groups (Fig. 5C,F) (unpaired t-test, t-value = 0.356; $P = 0.721$).

When the primary antibody was omitted from the PEG procedure, only two asymmetric synapses out of 400 were associated with PEG presynaptically. The number of PEG particles associated with these presynaptic membranes was 1 for both cases. This outcome indicates that nonspecific binding of secondary antibodies to ultrathin sections is negligible.

Comparison of the encounter frequency with axo-spinous synapses in stratum radiatum of the CA1 reveals a small difference

Earlier studies (Saura et al., 2004) had shown that the synaptic currents in the CA1 field carried by the NMDARs are reduced within PS-cDKO brains and that this phenotype is evident by the second postnatal month. To determine whether the reduction of NMDAR-currents may be explained by a reduction of excitatory synapses, rather than the strength of individual synapses, we compared the relative density of axo-spinous asymmetric (presumably excitatory) synapses within stratum radiatum of the CA1 of the PS-cDKO and control mice. The same ultrathin sections that were collected for the analysis of NR2A-PEG immunolabeling were examined to collect a series of electron microscopic 2D images spanning the stratum radiatum of the dorsal CA1 from the PCL to the SLM. Nineteen to 35 images at a magnification of 20,000× were required to tile the strata spanning from the most proximal to the most distal portions of the apical dendrites of the CA1 pyramidal cells. As shown in an example for one PS-cDKO and control tissue (Fig. 7), micrographs taken from the middle portion of the stratum radiatum exhibited less fluctuation in the frequency of encounter with axo-spinous junction profiles, relative to the frequency values obtained for the proximal portion of apical dendrites, nearest PCL (laminar position 1), or SLM (toward laminar position >25). For each animal, eight adjacent, nonoverlapping images spanning the middle third, i.e., just dorsal to SLM and clearly away from the proximal dendrites (the laminar positions depicted by lighter bars in Fig. 7), were used to estimate the relative synapse densities of each animal (our comparisons are of relative values, because the calculations were based on frequency of encounter with synaptic profiles within single micrographs, and not based on the disector's method or 3D reconstructions). Contrary to our expectation, the average value obtained from four hippocampi of the PS-cDKO group was 28% greater than the average value obtained from three hippocampi of the control group, although this difference was only marginally significant (two-tailed t-test, $P = 0.054$; 0.74 ± 0.04 synapse profiles per μm^2 for the control; 0.95 ± 0.04 synapse profiles per μm^2 for the PS-cDKO group; Fig. 8A).

Frequency of encounter with profiles within 2D images can be influenced by the size and shape of the profile (Guillery, 2002; Mouton, 2002). To determine whether the increased encounter with spines within PS-cDKO tissue could be due to enlargement of spines, we measured the spine widths of 101 spine profiles of controls and 172 spine profiles of PS-cDKO residing within the same ultrathin sections. The analysis yielded no statistically significant difference in the mean value

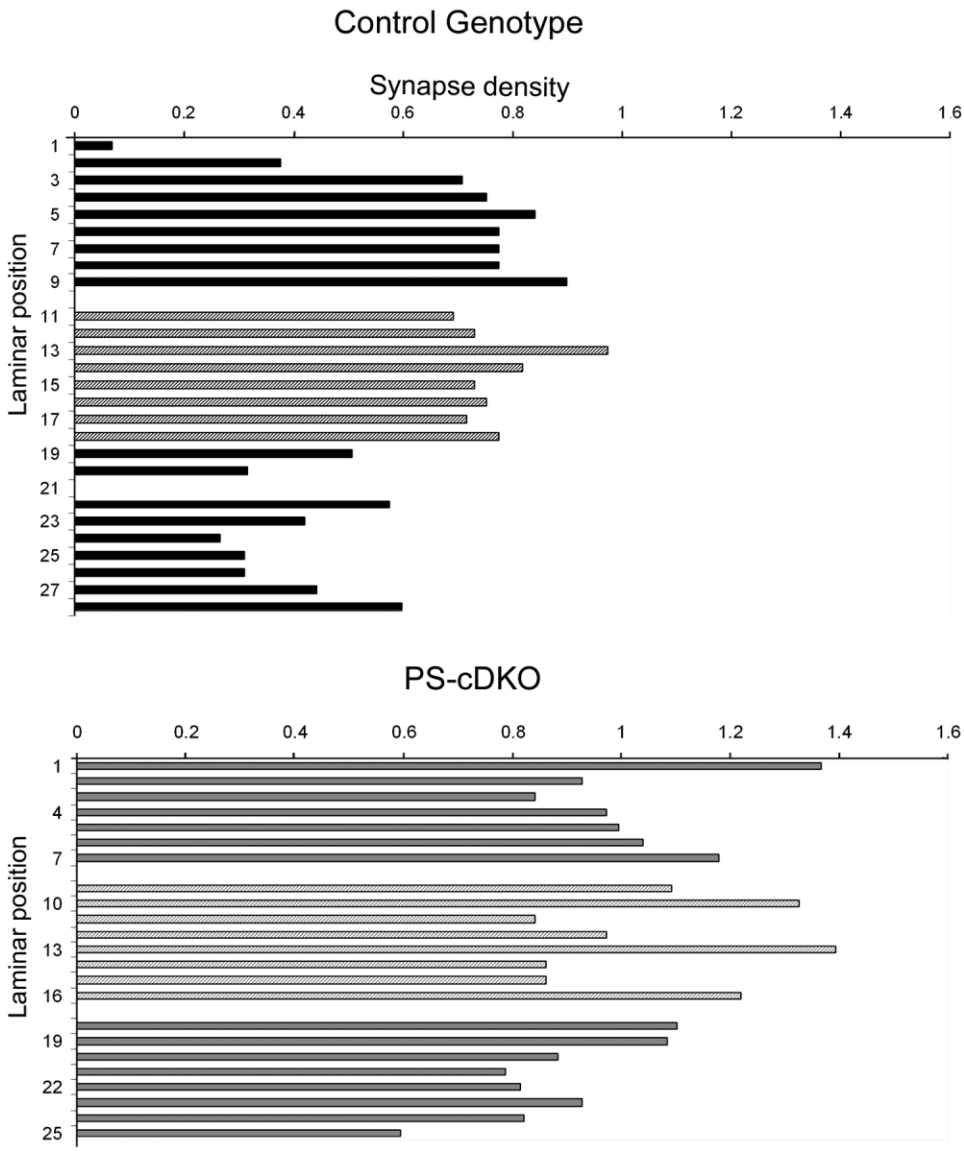

Figure 7.
Synapse analysis of the stratum radiatum of one control and one PS-cDKO depicts large variation in density. Each bar depicts the number of encounters with synaptic profiles within one electron micrograph spanning 45.385 μm^2. These are raw counts that have not undergone Abercrombie correction. The laminar position numbers indicate positions relative to the ventral edge of the pyramidal cell layer, with the most proximal position being Laminar position 1. The top panel summarizes the frequency of encounter with synaptic profile for one hippocampus of a control genotype, while the lower panel summarizes the frequency of encounter with synaptic profiles from one hippocampus of a PS-cDKO genotype.

($P = 0.40$; 251 ± nm for control; 264 ± 10 nm for the PS-cDKO) or distribution pattern of spine widths (Fig. 8B). The lack of difference in spine widths indicates that the apparent augmentation in the frequency of encounter with synaptic profiles within the PS-cDKO tissue could not be ascribed to the enlargement of individual spines.

DISCUSSION

This study was conducted to determine *how and why* the loss of PS function leads to the progressive, age-dependent neurodegeneration, inflammation, and reduction of synaptic plasticity as seen in AD (Hutton and Hardy, 1997; Beglopoulos et al., 2004; Saura et al., 2004; Shen and Kelleher, 2007). The outcome of the present study demonstrates that subtle but significant changes are emerging at the synaptic junction by the second postnatal month. Specifically, we observed that the proportion of dendritic spines in the stratum radiatum expressing NR2A is increased by 28% and this is compounded by a 31% increase in the level of NR2A precisely at the postsynaptic membrane. Placed against a background of zero spine loss, these findings indicate that NR2A levels at

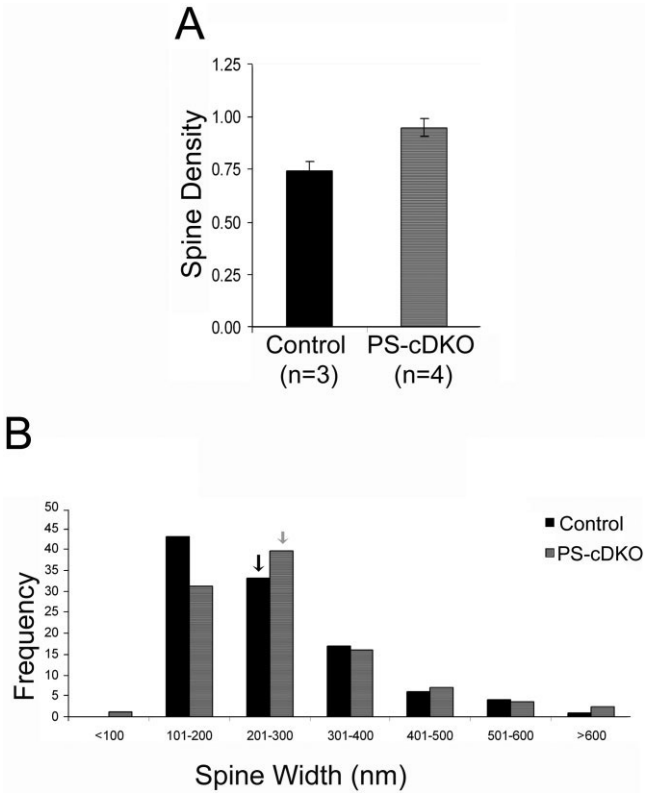

Figure 8.
Frequency of encounter with synaptic profiles in stratum radiatum of PS-cDKO hippocampus is not altered. Relative spine density in the stratum radiatum of the CA1 was assessed by analyzing 24 digitized images from three control animals and 32 images from four PS-cDKO animals (i.e., eight images per animal). Each image was captured at a magnification of 20,000×, spanning 45.385 μm^2 and approximately midway between the pyramidal cell layer and stratum lacunosum-moleculare. **A:** The frequency of encounter with asymmetric synaptic profiles is expressed as the mean of the number of encounter with synaptic profiles per μm^2 of synaptic area, after correcting for areas occupied by blood vessels or perikarya. This analysis indicates that synapse density is elevated in the CA1 field of the hippocampus of PS-cDKO animals, compared to the CA1 field of the hippocampus of controls, although this difference is only marginally significant ($P = 0.05$; $n = 3$ for control number of animals, and $n = 4$ for PS-cDKO number of animals). **B:** The distribution of spines (101 of controls, 172 of PS-cDKO spines), categorized according to their widths measured at widest portions captured within the same ultrathin sections used to count synapse density. Spine sizes are not significantly different across the genotypes (unpaired *t*-test, $P = 0.397$). Arrows point to the bin containing the mean values of the two genotype groups.

synapses become significantly elevated within 6 weeks following the postnatal deletion of presenilin 1 and 2. Our observation is consistent with the idea that NMDARs are trapped in the synaptic membrane, and this leads to excitotoxicity and the eventual neurodegeneration that is reported to become detectable by the sixth month in PS-cDKO brains (Saura et al., 2004).

In the same study (Saura et al., 2004), PS-cDKO was reported to cause a reduction in the input–output (I/O) field responses carried by NMDARs in hippocampal slices. This result reflects a change that could be pre- or postsynaptic. Based on the electrophysiological findings, we had expected to observe reduced levels of NMDAR subunits in spines of the stratum radiatum. Our new EM findings, namely, that the NR2A subunits at the synaptic junction are elevated, indicates that the reduced I/O ratio is not due to postsynaptic changes, such as the reductions in the synthesis of the NR2A subunit proteins that leads to reduced levels of NMDARs at the postsynaptic membrane. This observation is congruent with Saura et al.'s (2004) other biochemical finding, namely, that the levels of NR2A in cortical homogenates (which included the hippocampus) is not significantly different between the control and PS-cDKO genotypes.

Our EM findings suggest that the reduction in the I/O ratio carried by NMDARs could be due, primarily, to presynaptic changes (input) more than in the output carried by NMDARs. One possibility is that the coupling between axon depolarization (measured as fiber volley amplitude) and glutamate release (not measured) is reduced, thereby requiring greater input to evoke comparable amplitudes of NMDAR currents in the PS-cDKO hippocampus. For example, in the CA3 field of the hippocampus, presynaptic kainate receptors have a direct bidirectional effect on fiber volley amplitude and this change is not paralleled by changes in glutamate release (Schmitz et al., 2001). The EM data additionally show that, in spite of the elevated levels of NR2A subunits at synapses and the increased density of asymmetric (presumably excitatory) synapses, these augmentations are apparently not sufficient to compensate fully for the presynaptic changes revealed by the I/O field responses.

By now it is widely recognized that axons in the CA1 and elsewhere within the CNS also express a variety of presynaptic ionotropic receptors (MacDermott et al., 1999). The current and past EM-ICC data indicate that, indeed, both the NR2A and NR2B subunits occur within presynaptic axon terminals forming axo-spinous synapses in the CA1 field, as observed previously for the cortex (Aoki et al., 1994; Corlew et al., 2007) and hippocampus (Madara and Levine, 2008). Elevated levels of presynaptic NMDARs have been shown to contribute to enhancement in the timing-dependent long-term depression (LTD) that is characteristic of developing cortex (Corlew et al., 2007). The intracellular pathways that subserve synaptic plasticity in the developing cortex may also be present within the hippocampus of PS-cDKO brains. If so, the prevalence of presynaptic NR2A and of the timing-dependent LTD may contribute to mild impairment in spatial memory that is observed at this age (Saura et al., 2004).

Another possible explanation for the mismatch between the previous biophysical results and our current EM-ICC results is that the ratio of the phospho/dephosphorylation of NMDAR subunits is different. The antibodies we employed do not discriminate among the variable phosphorylation states of the NMDAR subunits, while biophysical measurements could be sensitive to the phosphorylation states of the receptor subunits. Saura et al. (2004) reported that the α-isoform of CaMKII is reduced specifically in the synaptoneurosome fraction of the PS-cDKO hippocampus. It would be interesting to find out whether this reduction of CaMKII could lead to the apparent reduction of NMDAR currents, even if levels of the protein are not reduced.

Saura et al. (2004) also reported LTP impairment by the second postnatal month among the PS-cDKO hippocampal slices. Our new findings allow us to conclude that impairment

of LTP in the hippocampus is probably not due to reduced levels of NMDAR. It is possible that LTP impairment is more tightly linked to reductions of CaMKII within the dendritic spines. Studies are under way to examine the impact of PS deletion on the localization of αCaMKII at varying stages of the AD-like symptoms in the PS-cDKO model of Alzheimer's disease.

LITERATURE CITED

Adams MM, Shah RA, Janssen WG, Morrison JH. 2001. Different modes of hippocampal plasticity in response to estrogen in young and aged female rats. Proc Natl Acad Sci U S A 98:8071–8076.

Adams MM, Fink SE, Janssen WG, Shah RA, Morrison JH. 2004. Estrogen modulates synaptic N-methyl-D-aspartate receptor subunit distribution in the aged hippocampus. J Comp Neurol 474:419–426.

Aoki C, Venkatesan C, Go CG, Mong JA, Dawson TM. 1994. Cellular and subcellular localization of NMDA-R1 subunit immunoreactivity in the visual cortex of adult and neonatal rats. J Neurosci 14:5202–5222.

Aoki C, Rodrigues S, Kurose H. 2000. Use of electron microscopy in the detection of adrenergic receptors. Methods Mol Biol 126:535–563.

Aoki C, Fujisawa S, Mahadomrongkul V, Shah PJ, Nader K, Erisir A. 2003. NMDA receptor blockade in intact adult cortex increases trafficking of NR2A subunits into spines, postsynaptic densities, and axon terminals. Brain Res 963:139–149.

Beglopoulos V, Sun X, Saura CA, Lemere CA, Kim RD, Shen J. 2004. Reduced beta-amyloid production and increased inflammatory responses in presenilin conditional knock-out mice. J Biol Chem 279: 46907–46914.

Bezprozvanny I, Mattson MP. 2008. Neuronal calcium mishandling and the pathogenesis of Alzheimer's disease. Trends Neurosci 31:454–463.

Corlew R, Wang Y, Ghermazien H, Erisir A, Philpot BD. 2007. Developmental switch in the contribution of presynaptic and postsynaptic NMDA receptors to long-term depression. J Neurosci 27:9835–9845.

Counts SE, Nadeem M, Lad SP, Wuu J, Mufson EJ. 2006. Differential expression of synaptic proteins in the frontal and temporal cortex of elderly subjects with mild cognitive impairment. J Neuropathol Exp Neurol 65:592–601.

Erisir A, Harris JL. 2003. Decline of the critical period of visual plasticity is concurrent with the reduction of NR2B subunit of the synaptic NMDA receptor in layer 4. J Neurosci 23:5208–5218.

Fujisawa S, Aoki C. 2003. In vivo blockade of N-methyl-D-aspartate receptors induces rapid trafficking of NR2B subunits away from synapses and out of spines and terminals in adult cortex. Neuroscience 121:51–63.

Guillery RW. 2002. On counting and counting errors. J Comp Neurol 447:1–7.

Hardy J, Selkoe DJ. 2002. The amyloid hypothesis of Alzheimer's disease: progress and problems on the road to therapeutics. Science 297:353–356.

Hutton M, Hardy J. 1997. The presenilins and Alzheimer's disease. Hum Mol Genet 6:1639–1646.

Kennedy MJ, Ehlers MD. 2006. Organelles and Trafficking Machinery for Postsynaptic Plasticity. Annu Rev Neurosci 29:325–362.

Kobayashi C, Aoki C, Kojima N, Yamazaki H, Shirao T. 2007. Drebrin a content correlates with spine head size in the adult mouse cerebral cortex. J Comp Neurol 503:618–626.

MacDermott AB, Role LW, Siegelbaum SA. 1999. Presynaptic ionotropic receptors and the control of transmitter release. Annu Rev Neurosci 22:443–485.

Madara JC, Levine ES. 2008. Presynaptic and postsynaptic NMDA receptors mediate distinct effects of brain-derived neurotrophic factor on synaptic transmission. J Neurophysiol 100:3175–3184.

Mouton PR. 2002. Principles and practices of unbiased stereology: an introduction for bioscientists. Baltimore: Johns Hopkins University Press.

Phend KD, Rustioni A, Weinberg RJ. 1995. An osmium-free method of epon embedment that preserves both ultrastructure and antigenicity for post-embedding immunocytochemistry. J Histochem Cytochem 43:283–292.

Rinaldi T, Kulangara K, Antoniello K, Markram H. 2007. Elevated NMDA receptor levels and enhanced postsynaptic long-term potentiation induced by prenatal exposure to valproic acid. Proc Natl Acad Sci U S A 104:13501–13506.

Saura CA, Choi SY, Beglopoulos V, Malkani S, Zhang D, Shankaranarayana Rao BS, Chattarji S, Kelleher RJ 3rd, Kandel ER, Duff K, Kirkwood A, Shen J. 2004. Loss of presenilin function causes impairments of memory and synaptic plasticity followed by age-dependent neurodegeneration. Neuron 42:23–36.

Schmitz D, Mellor J, Frerking M, Nicoll RA. 2001. Presynaptic kainate receptors at hippocampal mossy fiber synapses. Proc Natl Acad Sci U S A 98:11003–11008.

Selkoe DJ. 2002. Alzheimer's disease is a synaptic failure. Science 298: 789–791.

Shen J, Kelleher RJ 3rd. 2007. The presenilin hypothesis of Alzheimer's disease: evidence for a loss-of-function pathogenic mechanism. Proc Natl Acad Sci U S A 104:403–409.

Steiner H, Duff K, Capell A, Romig H, Grim MG, Lincoln S, Hardy J, Yu X, Picciano M, Fechteler K, Citron M, Kopan R, Pesold B, Keck S, Baader M, Tomita T, Iwatsubo T, Baumeister R, Haass C. 1999. A loss of function mutation of presenilin-2 interferes with amyloid beta-peptide production and notch signaling. J Biol Chem 274:28669–28673.

Thomas CG, Miller AJ, Westbrook GL. 2006. Synaptic and extrasynaptic NMDA receptor NR2 subunits in cultured hippocampal neurons. J Neurophysiol 95:1727–1734.

Tovar KR, Westbrook GL. 1999. The incorporation of NMDA receptors with a distinct subunit composition at nascent hippocampal synapses in vitro. J Neurosci 19:4180–4188.

Yildirim M, Janssen WG, Tabori NE, Adams MM, Yuen GS, Akama KT, McEwen BS, Milner TA, Morrison JH. 2008. Estrogen and aging affect synaptic distribution of phosphorylated LIM kinase (pLIMK) in CA1 region of female rat hippocampus. Neuroscience 152:360–370.

Yu H, Saura CA, Choi SY, Sun LD, Yang X, Handler M, Kawarabayashi T, Younkin L, Fedeles B, Wilson MA, Younkin S, Kandel ER, Kirkwood A, Shen J. 2001. APP processing and synaptic plasticity in presenilin-1 conditional knockout mice. Neuron 31:713–726.

Zarow C, Lyness SA, Mortimer JA, Chui HC. 2003. Neuronal loss is greater in the locus coeruleus than nucleus basalis and substantia nigra in Alzheimer and Parkinson diseases. Arch Neurol 60:337–341.